Texture evolution of ferroelectric AlScN films on metal under-layers

Minghua Li
Institute of Microelectronics
*Agency for Science, Technology and Research (A*STAR)*Singapore
li_minghua@ime.a-star.edu.sg

Huamao Lin
Institute of Microelectronics
*Agency for Science, Technology and Research (A*STAR)*
Singapore
lin_huamao@ime.a-star.edu.sg

Ping Luo
Institute of Materials Research and Engineering
*Agency for Science, Technology and Research (A*STAR)*
Singapore
luo_ping@ime.a-star.edu.sg

Kan Hu
Institute of Microelectronics
*Agency for Science, Technology and Research (A*STAR)*
Singapore
hu_kan@ime.a-star.edu.sg

Chen Liu
Institute of Microelectronics
*Agency for Science, Technology and Research (A*STAR)*
Singapore
liu_chen@ime.a-star.edu.sg

Li Chen
Institute of Microelectronics
*Agency for Science, Technology and Research (A*STAR)*
Singapore
chen_li@ime.a-star.edu.sg

Yao Zhu
Institute of Microelectronics
*Agency for Science, Technology and Research (A*STAR)*
Singapore
zhuya@ime.a-star.edu.sg

***Abstract* — Ferroelectric domain structure and the polarity inversion highly depend on the thin film texture. In this study, we deposited the AlScN films on various metal under-layers, and evaluated their microstructure. On the bottom metal surface, the initial AlScN exhibits poorer texture. When the film grows thicker, the grains become bigger and their orientation aligns better. The scandium concentration and the under metals properties play important roles for the initial AlScN layer formation. Two-stage texture evolution is proposed to understand the AlScN film growth, as well as the impacts of the scandium doping concentration and the metal under-layers.**

Keywords—scandium doped aluminum nitride, metal under-layers, texture, nucleation

I. Introduction

Excellent ferroelectric switching has been experimentally demonstrated on scandium doped aluminium nitride (AlScN) thin films containing Sc of 10 – 43 at. % [1 - 4]. The remnant polarization and the polarity inversion voltage strongly depend on Sc doping concentration and film deposition conditions. The as-deposited AlScN films exhibit good Wurtzite (0002) orientation, which facilitates the abrupt polarity inversion in the hysteresis loop [5]. Thanks to the matured and CMOS compatible integration technology, AlScN-based novel devices have also been designed and fabricated [6, 7].

The coercive field E_c of the AlScN-based ferroelectric switching ranges from 7 to 2 MV/cm, corresponding to the Sc concentration from 20 % to 40 %. This large E_c would benefit the device reliability. However compared to PZT film, (whose E_c ranges from 200 to 800 kV/cm depends on the film thickness [8]), the high operation voltage would hinder applications of the AlScN films.

To reduce the ferroelectric switching voltage, several approaches have been reported. Firstly, high scandium doping decreases the E_c due to its lower lattice constants *c*/*a* ratio [1, 9]. Second, using ultrathin film to reduce to switching voltage [5]. Stress engineering is another promising method. Lower coercive field was achieved in a tensile film [10]. Other doped AlN film like $Al_{1-x}B_xN$ [11] was also explored.

High scandium doping leads to poorer crystalline texture and more compressive stress [12]. The same trend is applicable when the film thickness reduces [13]. The challenge for the AlScN-based ferroelectric study is to simultaneously achieve high scandium doping, sub-20 nm thickness, and good (0002) crystallographic orientation. In this study, we evaluate the microstructure of different AlScN film samples on metal under layers. Our investigation on the film texture evolution provide an insight to the ferroelectric AlScN thin film optimization.

II. Experimental

A. AlScN film deposition

The substrates were 200 mm Si (100) wafers. Before AlScN film, the metal under-layer, either Ti (15 nm)/Pt (100 nm) or AlN (20 nm)/Mo (200 nm) was deposited. The crystalline quality of these metal films is essential for the AlScN growth.

Three kinds of AlScN films were fabricated, containing 20, 30, and 40 at. % of Sc respectively. They are referred to AlSc20N, AlSc30N, and AlSc40N hereafter. Two pulsed DC reactive magnetron sputtering chambers were utilized to deposit the AlScN films. AlSc20N films were sputtered in the single target chamber from an AlSc alloy target, while AlSc30N and AlSc40N films were grown in a co-sputtering chamber. The thickness of all AlScN films are 100 nm.

B. Film characterization

X-ray diffraction (XRD) 2θ - ω scans and rocking curves were recorded to evaluate the crystalline phase and the crystallographic alignment. High-resolution Transmission electron microscope (TEM) was used to inspect cross sections of the film stacks. A Focused Ion Beam (FIB) tool was utilized to prepare the cross sectional lamella for TEM observations.

This work was supported by the Science and Engineering Research Council of A*STAR (Agency for Science, Technology and Research), Singapore (Grant No. A20G9b0135).

III. Results and Discussion

A. XRD characterization

XRD 2θ - ω diffraction patterns are presented in Fig. 1a and 1b. Only the Wurtzite phase (0002) peak at 2θ ~ 36° is detected for all as-deposited AlScN films, demonstrating that our as-deposited AlScN films are highly *c*-axis textured. In addition, Pt (111) and Mo (110) peaks are also presented in the corresponding film stacks.

The average AlScN crystallite size can be estimated using the Full-Width-Half-Maximum (FWHM) of the (002) diffraction peak, by following Schetter equation [14]

$$D(2\theta) = \frac{K\lambda}{B\cos\theta} \quad (1)$$

where D and B are the average crystallite size and the FWHM of the diffraction peak. K is a dimensionless shape factor which typically equals to 0.9. θ is the Bragg angle, and λ represents the X-ray wavelength (1.5406 Å). Table I lists the (0002) peak locations and the calculated mean crystallite sizes.

Fig. 1c and 1d show the rocking curves of the AlScN (0002) reflection peaks. The FWHM measures the crystallographic alignment of the grains. A narrower peak indicates better crystallinity. We extracted the rocking curve RC-FWHM results as listed in Table I. The crystallites become smaller and the RC-FWHM is wider as the Sc concentration increases, indicating that the Sc doping makes the film crystallinity poorer. On the other hand, the film grown on Pt under-layer shows better texture than that on Mo.

B. TEM characterization

TEM cross-sectional image of the AlSc20N/Mo shows the AlScN columnar texture with nanometer size polycrystalline grains (Fig. 2a). Relative large and straight grains present at the top part of the film, while small grains were found in the film close to the bottom Mo. This two-stage film texture evolution was observed in all samples. In the following sessions, bulk growth and initial growth are used to denote the two stages respectively.

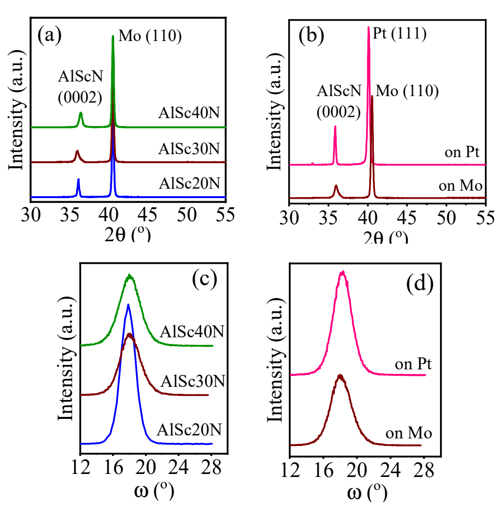

Fig. 1. XRD patterns of the 100 nm as-deposited AlScN films (a) with different Sc%, and (b) on different metal under-layers. (c) and (d) XRD rocking curves of the AlScN (0002) peaks.

TABLE I. SUMMARY OF XRD AND TEM RESULTS

	AlSc20N	AlSc30N	AlSc30N	AlSc40N
Metal under-layer	Mo	Mo	Pt	Mo
AlScN (0002) peak 2θ (°)	36.13	36.00	35.95	36.42
Average AlScN crystallite size (nm)	39	18	28	20
Rocking curve FWHM (°)	2.0	2.9	2.5	3.0
Film thickness at the initial stage (nm)	8-10	15-20	10-15	25-30

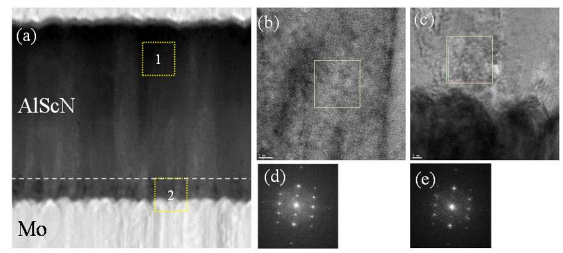

Fig. 2. (a) TEM cross-sectional view of the AlSc20N/Mo film stack. (b) & (c) high-resolution TEM images of the bulk and the initial AlScN film, as marked by Boxes 1&2 in (a). (d) & (e) corresponding FFT patterns of (b) and (c).

High-resolution TEM and Fast-Frourie-Transformation (FFT) studies were performed on the two regions where marked by the yellow boxes in Fig. 3a. The bulk film in Region 1 exhibits large crystalline grains and good (0002) alignment (Fig. 2b). Conversely in Region 2, the initial AlScN exhibits poorer texture, evidenced by the small tilt grains and the broadened FFT spots (Fig. 2c). Note there is no amorphous transition layer formed at the interface between the AlScN and the bottom metal, demonstrating direct AlScN nucleation on the bottom Mo surface. Based on the TEM images we determined the thicknesses of the initial stage for all samples (Table I). Larger thickness of the initial stage is found when the Sc % becomes higher. This finding provides a new angle to understand the complexity of the high Sc% AlScN film growth. The small AlScN grains and the poor texture at the initial stage would contribute to the surface energy states formation, and therefore modulate the charge transport characteristics [13].

To further study the metal under-layer impact, we have prepared two Mo under-layers with different surface conditions. The Root Mean Square (RMS) roughness values were controlled to be 1.2 and 0.4 nm for the rough and the smooth Mo surfaces, respectively. Fig. 3 presents the cross sectional TEM images of AlScN/Mo stacks. On the rough Mo surface, the AlScN initiates with the grains growth along diverse directions. A blurry and thicker interface between the AlScN and the rough Mo was observed. Conversely, the epitaxial-like AlScN initial growth was realized on the smooth Mo surface. Our finding confirmed that the smooth under-layer promotes the AlScN nucleation.

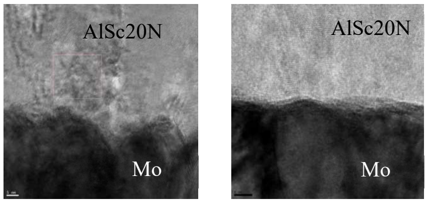

Fig. 3. The cross-sectional TEM images of the AlSc20N films grown on rough Mo surface (left) and on smooth Mo surface (right).

C. *Understanding AlScN film texture evolution*

Fig. 4 elaborates the two-stage AlScN texture evolution by referring to the classic crystallization process [15]. The heterogeneous nucleation leads to poor alignment of the initial AlScN crystallites. At the bulk growth stage, the evolutionary selection drives the columnar AlScN grains grow laterally and vertically with better (0002) crystallographic orientation (Fig. 4a). More Sc atoms incorporation increases the AlScN lattice deformation, which should be responsible for its larger initial thickness and the poorer film texture.

The rough under-layer surface causes extra challenge for the AlScN growth at the initial stage. More unpredicted nucleation generates smaller crystallites with diverse crystallographic orientation. Additional coarsening step is necessary and the gradual texture evolution is expected (Fig. 4b).

IV. Conclusions

We propose two-stage AlScN texture evolution process based on our findings. At the initial stage, the film consists of small tilt grains while at the bulk stage the AlScN grains grow larger and align better. As the film thickness scaling down, the initial stage would have more dominating effect.

As the Sc% increases, the interface between the AlScN and the metal under-layer becomes blurry and the initial growth layer becomes thicker. Moreover, on the rough surface of the metal under-layer, an additional coarsening step results in gradual AlScN texture evolution.

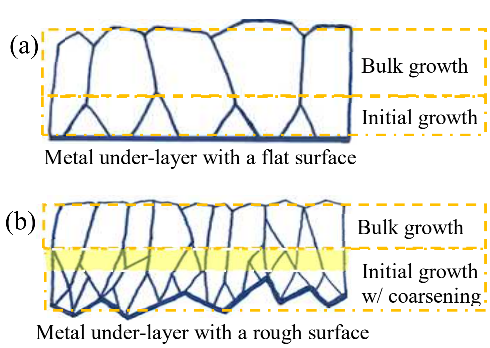

Fig. 4. Schematic diagrams showing the two-stage texture evolution of the AlScN film on (a) a flat and (b) a rough metal under-layer.

References

[1] S. Fichtner, N. Wolff, F. Lofink, L. Klenie, and B. Wagner, "AlScN: A III-V semiconductor based ferroelectric," J. Appl. Phys., vol. 125, pp. 114103, March 2019.

[2] D. Wang, J. Zheng, P. Musavigharavi, W. Zhu, A. C. Foucher, S. E. Trolier-McKinstry, E. A. Stach, and R. H. Olsson III, "Ferroelectric switching in sub-20 nm aluinum scandium nitride thin films", IEEE Electron Device Lett., vol. 41, pp. 1774-1777, December 2020.

[3] P. Wang, D. Wang, N. M. Vu, T. Chiang, J. T. Heron, and Z. Mi, "Fully epitaxial ferroelectric ScAlN growth by molecular beam epitaxy", Appl. Phys. Lett., vol. 118, pp. 223504, June 2021.

[4] C. Liu, Q. Wang, W. Yang, T. Cao, L. Chen, M. Li, F. Liu, D. K. Loke, J. Kang, and Y. Zhu, "Multiscale modeling of $Al_{0.7}Sc_{0.3}N$-based FeRAM: the steep switching, leakage and selector-free array", Proc. 2021 IEEE Int. Electron Devices Meeting (IEDM), USA, 2021.

[5] S. Yasuoka, T. Shimizu, A. Tateyama, M. Uehara, H. Yamada, M. Akiyama, Y. Hiranaga, Y. Cho, and H. Funakubo, "Effects of deposition conditions on the ferroelectric properties of $(Al_{1-x}Sc_x)N$ thin films", J. Appl. Phys., vol. 128, pp. 114103, September 2020.

[6] J. Wang, M. Park, S. Mertin, T. Pensala, F. Ayazi, and A. Ansari, "A film bulk acoustic resonator based on ferroelectric aluminum scandium nitride films", J. Microelectromech. Systems, vol. 29, pp. 741, October 2020.

[7] X. Liu, J. Zhengm D. Wang, P. Musavigharavi, E. A. Stach, R. Olsson III, and D. Jariwala, "Aluminum scandium nitride-based metal-ferroelectric-metal diode memory devices with high on/off ratios", Appl. Phys. Letter., vol. 118, pp. 202901, May 2021.

[8] N. A. Pertsev, J. R. Contreras, V. G. Kukhar, B. Hermanns, H. Kohlstedt, and R. Waser, "Coercive field of ultrathin $Pb(Zr_{0.52}Ti_{0.48})O_3$ epitaxial films", Appl. Phys. Lett., vol. 83, pp. 3356-3358, August 2003.

[9] H. Wang, N. Adamski, S. Mu, and C. G. van de Walle, "Piezoelectric effect and polarization switching in $Al_{1-x}Sc_xN$", J. Appl. Phys., vol. 130, pp. 104101, August 2021.

[10] K. Yazawa, D. Drury, A. Zakutayev, and G. L. Brennecka, "Reduced coercive field in epitaxial thin film of ferroelectric wurtzite $Al_{0.7}Sc_{0.3}N$", Appl. Phys. Lett., vol. 118, pp. 162903, March 2021.

[11] W. Zhu, J. Hayden, F. He, J. –I. Yang, P. Tipsawat, M.D. Hossain, J. –P. Maria, and S. Trolier-McKinstry, "Strongly temperature dependent ferroelectric switching in AlN, $Al_{1-x}Sc_xN$, and $Al_{1-x}B_xN$ thin films", Appl. Phys. Lett., vol. 119, pp. 062901, July 2021.

[12] S. Fichner, T. Reimer, S. Chemnitz, F. Lofink, and B. Wagner, "Stress controlled pulsed direct current co-sputtered $Al_{1-x}Sc_xN$ as piezoelectric phase for micromechanical sensor applications", APL Mater., vol. 3, pp. 116102, November 2015.

[13] K. Knisely, E. Douglas, J. Mudrick, M. Rodriguez, and P. Kotula, "Thickness dependence of Al0.88Sc0.12N thin films grown on silicon", Thin Solid Films, vol. 675, pp. 66-72, February 2019.

[14] U. Holzwarth, and N. Gibson, "The Scherrer equation versus the 'Debye-Scherrer equation'", Nature Nanotechnology., vol. 6, pp. 534, September. 2011.

[15] J. J. De Yoreo, and P. G. Vekilov, "Principles of crystal nucleation and growth", Rev. Mineralogy Geochem., vol 54, pp. 57-93, January 2003.